Monthly Notices
of the
ROYAL ASTRONOMICAL SOCIETY

MNRAS **481,** 4250–4260 (2018)
Advance Access publication 2018 September 18

doi:10.1093/mnras/sty2547

Hard X-ray-selected giant radio galaxies – I. The X-ray properties and radio connection

F. Ursini ,[1]★ L. Bassani,[1] F. Panessa,[2] A. J. Bird ,[3] G. Bruni ,[2] M. Fiocchi,[2] A. Malizia,[1] L. Saripalli[4] and P. Ubertini[2]

[1]*INAF – Osservatorio di Astrofisica e Scienza dello Spazio di Bologna, Via Piero Gobetti 93/3, I-40129 Bologna, Italy*
[2]*INAF – Istituto di Astrofisica e Planetologia Spaziali, via Fosso del Cavaliere 100, I-00133 Roma, Italy*
[3]*School of Physics and Astronomy, University of Southampton, SO17 1BJ, UK*
[4]*Raman Research Institute, C. V. Raman Avenue, Sadashivanagar, Bangalore 560080, India*

Accepted 2018 September 11. Received 2018 September 1; in original form 2018 July 13

ABSTRACT

We present the first broad-band X-ray study of the nuclei of 14 hard X-ray-selected giant radio galaxies, based both on the literature and on the analysis of archival X-ray data from *NuSTAR*, *XMM–Newton*, *Swift*, and *INTEGRAL*. The X-ray properties of the sources are consistent with an accretion-related X-ray emission, likely originating from an X-ray corona coupled to a radiatively efficient accretion flow. We find a correlation between the X-ray luminosity and the radio core luminosity, consistent with that expected for active galactic nuclei powered by efficient accretion. In most sources, the luminosity of the radio lobes and the estimated jet power are relatively low compared with the nuclear X-ray emission. This indicates that either the nucleus is more powerful than in the past, consistent with a restarting of the central engine, or that the giant lobes are dimmer due to expansion losses.

Key words: galaxies: active – galaxies: nuclei – galaxies: Seyfert – X-rays: galaxies.

1 INTRODUCTION

Active galactic nuclei (AGNs) are powerful sources emitting across all the electromagnetic spectrum. Their central engine is thought to be a supermassive black hole surrounded by an accretion disc, mostly emitting in the optical/ultraviolet band. The X-ray emission is thought to originate, at least in radio-quiet AGNs, via Comptonization of disc photons in a hot corona (e.g. Haardt & Maraschi 1991; Haardt, Maraschi & Ghisellini 1994, 1997). The primary X-ray emission can be absorbed by the circumnuclear material, and also Compton reflected by the disc (e.g. George & Fabian 1991; Matt, Perola & Piro 1991) or the torus at pc scales (e.g. Ghisellini, Haardt & Matt 1994; Matt, Guainazzi & Maiolino 2003). In radio galaxies, powerful jets are also observed, producing radio through gamma radiation via synchrotron and synchrotron self-Compton mechanisms. From the seminal work of Fanaroff & Riley (1974), radio galaxies are divided into two subclasses according to their morphology and radio power: the low-power Fanaroff–Riley (FR) I and the high-power FR II. FR Is are more compact and their radio luminosity peaks near the nucleus, while FR IIs exhibit well-separated radio lobes with bright outer edges. When jets are observed, they are more collimated in FR IIs. Also the origin of the X-ray emission is likely different between the two classes, being mostly related to the jet in FR Is (e.g. Balmaverde, Capetti & Grandi 2006; Hardcastle, Evans & Croston 2009; Mingo et al. 2014) and to the accretion disc/corona system in FR IIs (e.g. Grandi, Malaguti & Fiocchi 2006).

Giant radio galaxies (GRGs) are the largest (linear size >0.7 Mpc) single objects in the Universe, and represent an extreme class among radio-loud AGNs. Their extraordinary size, extending well beyond the host galaxy, makes them ideal targets to study the large-scale structure of the Universe and probe the warm-hot intergalactic medium (Malarecki et al. 2013, 2015). Moreover, according to the evolution models of radio galaxies (e.g. Kaiser & Alexander 1999; Hardcastle & Krause 2013), GRGs should be very old and/or residing in a very low-density environment compared with regular radio galaxies (e.g. Subrahmanyan, Saripalli & Hunstead 1996; Mack et al. 1998; Machalski, Chyzy & Jamrozy 2004; Malarecki et al. 2015). The origin and growth of GRGs is still an open issue, and could be related to the restarting of their central engines during multiple activity phases (e.g. Subrahmanyan et al. 1996). Also the environment can be an important factor, since the radio lobes tend to grow to giant sizes towards low-density regions (Malarecki et al. 2015); in particular, the radio axes of GRGs are preferentially closer to the minor axes of the host galaxies (Saripalli & Subrahmanyan 2009).

So far, around 300 GRGs have been reported in the literature, mostly from radio surveys (Wężgowiec, Jamrozy & Mack 2016, and references therein). Their discovery is challenging because, despite their huge total energy content, their large volume implies a very low energy density and a very low surface brightness, thus

★ E-mail: francesco.ursini@inaf.it

Table 1. The GRGs analysed in this work, with the list of X-ray data used here and radio data with corresponding references.

Name	z	Optical class	Galactic $N_{\rm H}$ (10^{20} cm^{-2})	$\log M_{\rm BH}$	X-ray data	Radio data	Ref.
0318+684	0.090100	Sy1.9	30.8	–	*XMM*+*NuSTAR*+BAT+IBIS	*VLA*	Lara et al. (2001)
PKS 0707−35	0.110800	Sy2	17.0	–	*NuSTAR*+BAT	*ATCA*	Saripalli et al. (2013)
Mrk 1498	0.054700	Sy1.9	1.8	8.59	*XMM*+*NuSTAR*+BAT	*VLA*	Schoenmakers et al. (2000a)
PKS 2331−240	0.047700	Sy1.8	1.6	8.75	*XMM*+*NuSTAR*+BAT	*VLA*	Hernández-García et al. (2017)
PKS 2356−61	0.096306	Sy2	1.5	8.96	*NuSTAR*+BAT	*ATCA*	Subrahmanyan et al. (1996)

Table 2. The GRGs with X-ray data taken from the literature, with radio data and corresponding references.

Name	z	Optical class	$\log M_{\rm BH}$	X-ray data	Ref.	Radio data	Ref.
B3 0309+411b	0.134000	Sy1	–	*XMM*+BAT+IBIS	Molina et al. (2008)	*VLA*	Schoenmakers et al. (2000a)
4C 73.08	0.058100	Sy2	–	*XMM*+*NuSTAR*	Ursini et al. (2018a)	*VLA*	Lara et al. (2001)
HE 1434−1600	0.144537	BLQSO	8.64	*Swift*/XRT+BAT	Panessa et al. (2016)	*VLA*	Letawe et al. (2004)
IGR J14488−4008	0.123	Sy1.5	8.58	*XMM*+BAT+IBIS	Molina et al. (2015)	*GMRT*	Molina et al. (2015)
4C 63.22	0.20400	Sy1	–	*Swift*/XRT+BAT	Panessa et al. (2016)	*VLA*	Lara et al. (2001)
4C 34.47	0.20600	Sy1	8.01	*XMM*+BAT	Ricci et al. (2017)	*WSRT*	Jagers et al. (1982)
IGR J17488−2338	0.240	Sy1.2	9.11	*XMM*+IBIS	Molina et al. (2014)	*VLA*	Molina et al. (2014)
PKS 2014−55	0.060629	Sy2	–	*Swift*/XRT+BAT	Panessa et al. (2016)	*ATCA*	Saripalli et al. (2007)
4C 74.26	0.10400	Sy1	9.37	*XMM*+BAT+IBIS *NuSTAR*+XRT	Molina et al. (2008) Lohfink et al. (2017)	*VLA*	Lara et al. (2001)

requiring sensitive radio telescopes. Another problem is the large angular size, which makes it difficult to distinguish the real radio structure from physically unrelated sources. Indeed, in the complete sample of Revised Third Cambridge Catalogue of Radio sources (3CR) extragalactic radio sources (Laing, Riley & Longair 1983), only around 6 per cent of them are found to be giant, and this fraction is only 1 per cent at redshift $z < 1$ (Ishwara-Chandra & Saikia 1999). Among the radio galaxies of the more sensitive Australia Telescope Low Brightness Survey Extended Sources Sample, around 12 per cent are candidate giants, with about 3 per cent being giants at $z < 1$ (Saripalli et al. 2012).

Recently, Bassani et al. (2016) extracted a sample of 64 AGNs with extended radio morphology from the hard X-ray catalogues of *INTEGRAL*/IBIS (Malizia et al. 2012) and *Swift*/BAT (Baumgartner et al. 2013). Surprisingly, the fraction of GRGs was found to be 22 per cent, i.e. significantly larger than what is generally found in radio surveys. Also, 60 per cent of objects were found to have linear sizes above 0.4 Mpc. It is still unclear why the hard X-ray selection favours the detection of giant radio sources. This could be partly due to observational biases that prevent the detection of GRGs in radio surveys. However, hard X-ray-selected AGNs are also biased towards luminous and highly accreting sources; this could in turn suggest that hard X-ray-selected radio galaxies are those with a central engine powerful enough to produce giant radio structures (for a detailed discussion, see Bassani et al. 2016).

In this paper, we discuss for the first time the broad-band X-ray properties of a sample of hard X-ray-selected GRGs, and more specifically of the 14 GRGs selected in Bassani et al. (2016), and investigate their connection with the radio emission. To this aim, we gathered information either from the literature or by direct analysis of archival X-ray data, focusing in particular on *NuSTAR*. A study of the radio morphology and evolution of these sources will be presented in a forthcoming work (Bruni et al., in preparation). The structure of the paper is as follows. In Section 2, we present the sample of hard X-ray-selected GRGs. In Section 3, we present the X-ray observations analysed in this work. We discuss the results in Section 4, and summarize the conclusions in Section 5.

2 THE SAMPLE

We collected X-ray data for all the 14 radio galaxies reported as giants in Bassani et al. (2016), namely showing a linear extent above 0.7 Mpc (for $H_0 = 71$ km s^{-1} Mpc^{-1}, $\Omega_{\rm and} = 0.27$, $\Omega_\Lambda = 0.73$). All these sources display an FR II radio morphology. The sample includes local AGNs ($z \lesssim 0.2$) of different optical classes, type 1 and 2 objects being equally represented (see Tables 1 and 2). We also collected the available information on the radio fluxes from the literature, mostly relying on high-resolution (5–45 arcsec) 1.4 GHz data that allowed disentangling the different contributions from the core and the lobes. Concerning the X-ray data, we focused on broad-band spectra including *INTEGRAL*/IBIS and/or *Swift*/BAT at high energies (14–195 keV), and *XMM–Newton*, *Chandra* or *Suzaku* at lower energies (0.3–10 keV). For 3 sources out of 14, only *Swift*/XRT data are available, and have been analysed in Panessa et al. (2016). As of 2018 April, seven sources have been observed by *NuSTAR* in targeted observations, whose data either are published or will be discussed in the following. The basic data of the five sources analysed in this work, together with their radio observations, are reported in Table 1. The data of the nine sources with X-ray information taken from the literature are reported in Table 2. The black hole masses were collected by Panessa et al. (2016), to whom we refer the reader for the details; the mass of PKS 2331−240 was estimated from the stellar velocity dispersion by Hernández-García et al. (2017).

3 *NuSTAR* OBSERVATIONS, DATA REDUCTION AND ANALYSIS

NuSTAR (Harrison et al. 2013) observed 0318+684, PKS 0707−35, Mrk 1498, PKS 2331−240, and PKS 2356−61 as part of the *NuSTAR* extragalactic survey.

3.1 The sources

0318+684 is among the largest radio sources of our sample, having a linear size of 1.5 Mpc (Bassani et al. 2016). It hosts an AGN opti-

Table 3. Logs of the *NuSTAR* observations analysed in this work.

Source	Obs. ID	Start time (UTC) yyyy-mm-dd	Net exp. (ks)
0318+684	60061342002	2016-05-04	24
PKS 0707−35	60160285002	2016-11-24	19
Mrk 1498	60160640002	2015-05-11	24
PKS 2331−240	60160832002	2015-07-30	21
PKS 2356−61	60061330002	2014-08-10	23

cally classified as a Seyfert 1.9 (Véron-Cetty & Véron 2006). This source was also observed by *XMM–Newton* in 2006 and studied by Winter et al. (2008), who reported an X-ray absorbing column density of around 4×10^{22} cm^{-2} and an X-ray photon index $\Gamma_X \simeq 1.5$.

PKS 0707−35 has been classified as a type 2 source by Tazaki et al. (2013) from the X-ray obscuration ($N_H > 10^{22}$ cm^{-2}) observed with *Suzaku*. Tazaki et al. (2013) also reported $\Gamma_X \simeq 1.66$ and found the presence of a relatively weak reflection component compared with typical Seyfert galaxies. The radio morphology is complex, as it shows two distinct lobe pairs, offset from each other at an angle of 30°, indicating a restarting activity scenario (Saripalli et al. 2013).

Mrk 1498 is a peculiar source, optically classified as a Seyfert 1.9 (Véron-Cetty & Véron 2006), showing large-scale ionization cones in the optical band that are not aligned with the radio lobes, and that might be interpreted as due to a fading or obscured AGN (Keel et al. 2015, 2017). From *Suzaku* data, Eguchi et al. (2009) found an X-ray absorbing column density of a few $\times 10^{23}$ cm^{-2} and $\Gamma_X \simeq 1.8$, and suggested the obscuration is produced by a patchy torus. A multiwavelength study on this source will be presented in a forthcoming work (Hernandez-García et al., in preparation). Here, we focus on the *NuSTAR* data, complemented by a 2007 *XMM–Newton* observation.

PKS 2331−240 has a peculiar optical spectrum with variable broad emission lines. This source has been optically classified as a Seyfert 2 (Parisi et al. 2012) and later reclassified as a Seyfert 1.9 (Hernández-García et al. 2017), changing to type 1.8 in one year (Hernández-García et al. 2018). The radio morphology shows two giant lobes plus a blazar-like core in the centre, suggesting the jet has changed its orientation and is now pointing in our line of sight (Hernández-García et al. 2017). Concerning the X-ray spectrum, Panessa et al. (2016) reported $\Gamma_X \simeq 1.70$ and no intrinsic absorption from *Swift*/XRT+BAT data (see also Hernández-García et al. 2018). This object was also observed once by *NuSTAR* and twice by *XMM–Newton* in 2015, although never simultaneously. Hernández-García et al. (2017) reported $\Gamma_X \simeq 1.77$ and no intrinsic absorption from the *XMM–Newton* data.

Finally, PKS 2356−61 is a Seyfert 2 (Véron-Cetty & Véron 2006) and a very powerful radio galaxy, with large and bright hotspots (e.g. Subrahmanyan et al. 1996; Mingo et al. 2014, 2017). From *Chandra* data, Mingo et al. (2014) concluded that the X-ray spectrum is dominated by an accretion-related continuum, absorbed by a column density of around 1.5×10^{23} cm^{-2}. From the same data, Mingo et al. (2017) detected synchrotron X-ray emission from one of the hotspots.

3.2 The X-ray data

We report in Table 3 the logs of the archival *NuSTAR* data sets of the sources analysed here. Since *NuSTAR* is sensitive in the 3–79 keV band, it allows us to constrain the different X-ray spectral components, namely the primary power-law-like continuum, the Compton-reflection component producing a bump at 20–30 keV and the Fe Kα line at 6.4 keV. We included for all sources the *Swift*/BAT spectra (Barthelmy et al. 2005) to extend the coverage up to 195 keV, and also *INTEGRAL*/IBIS data (Ubertini et al. 2003) for 0318+684. We also included the soft X-ray spectra by *XMM–Newton* (Jansen et al. 2001) for 0318+684, Mrk 1498, and PKS 2331−240, to better constrain the absorbing column density and the Fe Kα line.

The *NuSTAR* data were reduced using the standard pipeline (NUPIPELINE) in the *NuSTAR* Data Analysis Software (NUSTARDAS, v1.8.0), using calibration files from *NuSTAR* CALDB v20180312. We extracted the spectra using the standard tool NUPRODUCTS for each of the two hard X-ray detectors, which reside in the corresponding focal plane modules A and B (FPMA and FPMB). We extracted the source data from circular regions with a radius of 75 arcsec, and the background from a blank area close to the source. The spectra were binned to have a signal-to-noise ratio larger than 3 in each spectral channel, and not to oversample the instrumental resolution by a factor greater than 2.5. The spectra from the two detectors were analysed jointly, but not combined.

The *XMM–Newton* data were processed using the *XMM–Newton* Science Analysis System (SAS v16.1). For simplicity, we used EPIC-pn data only, because of the much larger effective area compared with the MOS detectors and to avoid uncertainties due to cross-calibration issues. The source extraction radii and screening for high-background intervals were determined through an iterative process that maximizes the signal-to-noise ratio (Piconcelli et al. 2004). We extracted the background from circular regions with a radius of 50 arcsec, while the source extraction radii were in the range 20–40 arcsec. We binned the spectra to have at least 30 counts per spectral bin, and not oversampling the instrumental resolution by a factor greater than 3.

The *INTEGRAL* spectrum of 0318+684 consists of ISGRI data from several pointings between revolution 12 and 530 (from the fourth IBIS catalogue; Bird et al. 2010). The data extraction was carried out following the procedure described in Molina et al. (2013).

Finally, we included the average 105-month *Swift*/BAT spectra from the most recent hard X-ray survey (Oh et al. 2018).[1]

3.3 Spectral analysis

The spectral analysis was carried out with the XSPEC 12.10.0 package (Arnaud 1996), using the χ^2 minimization technique. All errors are quoted at the 90 per cent confidence level. We fitted the 3–79 keV *NuSTAR* spectra and the 14–195 keV *Swift*/BAT spectra simultaneously, leaving the cross-calibration constant C_{BAT} free to vary, after checking for consistency between the two instruments. We did the same for the 20–100 keV *INTEGRAL*/IBIS spectrum and included a cross-calibration constant C_{IBIS}. We also included a cross-calibration factor between *NuSTAR*/FPMA and FPMB, which is always consistent with unity and smaller than 1.02. The *XMM–Newton*/pn data allowed us to extend the analysis down to 0.3 keV for 0318+684, Mrk 1498 and PKS 2331−240. In these cases, we included a cross-calibration constant C_{pn} free to vary to account for flux variability between the different observations.

In our fits, we always included Galactic absorption, fixing the hydrogen column densities to the values obtained from the H I map of Kalberla et al. (2005), as given by the tool NH in the HEASOFT package. The values of Galactic N_H are reported in Table 1. For all

[1] https://swift.gsfc.nasa.gov/results/bs105mon/

Table 4. Best-fitting parameters of the X-ray spectra analysed in this work.

Name	Model	Γ_X	N_H (10^{22} cm^{-2})	E_c (keV)	$\mathcal{R}$	EW$_{K\alpha}$ (eV)	C_{pn}	C_{BAT}	C_{IBIS}	χ^2/dof
0318+684	B	1.40 ± 0.12	4.0 ± 0.3	60^{+60}_{-30}	<0.17	50 ± 40	2.0 ± 0.1	0.85 ± 0.15	1.3 ± 0.6	245/237
PKS 0707−35	A	1.6 ± 0.2	8^{+7}_{-6}	>90	<2	<350	–	3.0 ± 0.8	–	100/95
Mrk 1498	C	1.5 ± 0.1	23 ± 2	80^{+50}_{-20}	<0.35	90 ± 50	0.94 ± 0.04	1.00 ± 0.08	–	396/390
PKS 2331−240	A	1.91 ± 0.07	0.011 ± 0.003	>250	<0.3	<50	0.65 ± 0.07 0.54 ± 0.06	0.45 ± 0.12	–	611/540
PKS 2356−61	A	1.7 ± 0.3	14 ± 5	>55	<1.3	<170	–	0.9 ± 0.2	–	131/159

Table 5. X-ray spectral parameters of the sources reported in the literature.

Name	Γ_X	N_H (10^{22} cm^{-2})	E_c (keV)	$\mathcal{R}$	EW$_{K\alpha}$ (eV)	Ref.
B3 0309+411b	1.90 ± 0.08	–	–	>1.2	70 ± 40	1
4C 73.08	1.61 ± 0.17	40 ± 8	–	<2.2	120 ± 100	2
HE 1434−1600	1.72 ± 0.06	–	–	–	–	3
IGR J14488−4008	$1.71^{+0.16}_{-0.17}$	0.17 ± 0.04	67^{+227}_{-36}	1(f)	93^{+35}_{-34}	4
4C 63.22	1.96 ± 0.08	–	–	–	–	3
4C 34.47	1.98 ± 0.12	–	>97	$2.0^{+2.1}_{-1.6}$	–	5
IGR J17488−2338	1.37 ± 0.11	$1.14^{+0.26}_{-0.23}$	–	<1.8	128^{+61}_{-62}	6
PKS 2014−55	1.86 ± 0.21	32^{+12}_{-9}	–	–	–	3
4C 74.26	1.8–1.9	$\sim 0.35^a$	183^{+51}_{-35}	1.2 ± 0.7	90–200	7,8,9

Notes. [a]Ionized absorber. References: 1. Molina et al. (2008), 2. Ursini et al. (2018a), 3. Panessa et al. (2016), 4. Molina et al. (2015), 5. Ricci et al. (2017), 6. Molina et al. (2014), and 7. Molina et al. (2008), Di Gesu & Costantini (2016), Lohfink et al. (2017).

models, we adopted the chemical abundances of Anders & Grevesse (1989) and the photoelectric absorption cross-sections of Verner et al. (1996).

We first fitted the data with a model consisting of an absorbed power law plus a reflection component and a narrow Gaussian emission line. We used the PEXRAV model (Magdziarz & Zdziarski 1995) in XSPEC, which includes the continuum reflected off a neutral medium of infinite column density in a slab geometry. We always fixed the inclination angle at 60°, and we assumed solar abundances. We left free to vary the photon index Γ_X, the reflection fraction $\mathcal{R}$ and the high-energy cut-off E_c in PEXRAV. Since the energy of the Gaussian line was always poorly constrained, we fixed it at 6.4 keV (rest frame), i.e. that expected for neutral Fe Kα emission. In XSPEC notation, this baseline model reads: CONST*PHABS*ZPHABS*(PEXRAV + ZGAUSS), where CONST is the cross-calibration constant, PHABS is the fixed Galactic absorption, ZPHABS is the (redshifted) intrinsic absorption. This model is designated as Model A in the following.

When including pn data down to 0.3 keV, we noted a 'soft excess' on top of the absorbed power law, which is commonly observed in the X-ray spectra of type 2 AGNs (e.g. Turner et al. 1997; Guainazzi, Matt & Perola 2005). In radio-quiet Seyfert 2s, this excess is generally explained as optically thin scattered continuum (e.g. Turner et al. 1997; Ueda et al. 2007) and/or photoionized emission from circumnuclear gas (e.g. Guainazzi & Bianchi 2007). In obscured radio galaxies, on the other hand, the excess can be attributed to unabsorbed X-ray emission from the jet (e.g. Hardcastle et al. 2009; Mingo et al. 2014). In any case, the excess is generally well described by a power law. We thus included to the baseline model (Model A) a secondary, unabsorbed power law. In XSPEC notation, this model (Model B) reads: CONST*PHABS*[ZPHABS*(PEXRAV + ZGAUSS)+CONST2*POWERLAW]. If the soft excess is interpreted as a scattered component, then CONST2 would represent the scattered fraction f_s, which is generally of a few per cent or less (e.g. Turner et al. 1997). The parameters of the second power law are tied to those of PEXRAV. Finally, to test the presence of photoionized emission, we added a thermal component to Model B. We used the MEKAL model in XSPEC. Then, in XSPEC notation, this model (Model C) reads: CONST*PHABS*[ZPHABS*(PEXRAV + ZGAUSS + MEKAL)+CONST2*POWERLAW].

The results obtained for each source are discussed below and summarized in Table 4, where we report the main best-fitting parameters. The X-ray spectral parameters for the other sources in our sample have been collected from the literature and are reported in Table 5.

3.3.1 0318+684

NuSTAR observed this source in 2016 with a net exposure of 24 ks, while *XMM–Newton* observed the source in 2006 (Obs. Id. 0312190501) with a net exposure of 6.5 ks. As a consistency check, we fitted the *NuSTAR* and *XMM–Newton*/pn spectra in the common bandpass 3–10 keV with a simple power law. The photon index was found to be 1.26 ± 0.09 in *NuSTAR* and 1.2 ± 0.1 in pn, i.e. the spectral shape is consistent with being the same. On the other hand, the normalization measured by pn is a factor of 2 higher than in *NuSTAR*, indicating a flux variation between the two observations. However, the spectral shape being consistent, we fitted simultaneously the *NuSTAR* and pn spectra, also including *Swift*/BAT and *INTEGRAL*/IBIS to get the broadest energy band (0.3–195 keV).

Model A provides a decent fit to the data (χ^2/dof = 265/238), but leaves significant residuals in the soft band. The fit is improved using Model B (χ^2/dof = 245/237 and $\Delta\chi^2/\Delta$dof = −20/−1), and we obtain decent constraints on the intrinsic photon index and on the column density, as reported in Table 4. These results are consistent, within the errors, with those reported by Winter et al. (2008) from the analysis of the pn data alone. We only have an upper limit to the reflection fraction $\mathcal{R} < 0.17$, while the Gaussian line at 6.4 keV

has an equivalent width of $EW_{K\alpha} = 50 \pm 40$ eV. The high-energy cut-off is found to be $E_c = 60^{+60}_{-30}$ keV.

3.3.2 PKS 0707-35

Only *NuSTAR* and BAT data were available for this source, we thus fitted the spectra with the baseline Model A. We find a good fit with χ^2/dof = 100/95. The cross-calibration constant is large ($C_{BAT} = 3.0 \pm 0.8$), but leaving the photon index free to change between *NuSTAR* and BAT does not improve the fit. We only derive rough upper limits to the presence of a reflection component ($\mathcal{R} < 2$) and of the Fe Kα line ($EW_{K\alpha} < 350$ eV). We note that the 2–10 keV flux measured by *NuSTAR* is a factor of 4 less than that by *Suzaku* (5×10^{-12} erg s^{-1} cm^{-2}) as given in Tazaki et al. (2013).

3.3.3 Mrk 1498

This source was observed by *NuSTAR* in 2015 with a net exposure of 24 ks, and by *XMM–Newton* in 2007 (Obs. ID 0500850501) with a net exposure of 7.5 ks. Since the spectrum shows strong signatures of X-ray absorption, to check for consistency between *NuSTAR* and pn we proceeded as follows. We first fitted the 3–10 keV *NuSTAR* spectra with a simple power law modified by ZPHABS. We found a photon index 1.58 ± 0.13 and a column density of $(19 \pm 3) \times 10^{22}$ cm^{-2}. Then, we fitted the pn spectrum in the same energy band and with the same model, fixing the parameters and only allowing for a free cross-calibration constant. We found a good fit and $C_{pn} = 0.93 \pm 0.03$, indicating a good agreement between the two spectra. We fitted jointly the *NuSTAR*, pn and BAT spectra in the 0.3–195 keV band. Model A gives a very poor fit (χ^2/dof = 763/394). The fit is greatly improved using Model B (χ^2/dof = 428/392 and $\Delta\chi^2/\Delta$dof = −335/ −2), but with significant residuals in the soft band. Finally, Model C yields a good fit with no prominent residuals (χ^2/dof = 396/390 and $\Delta\chi^2/\Delta$dof = −32/ −2). We obtain a photon index of 1.5 ± 0.1, a column density of $(23 \pm 3) \times 10^{22}$ cm^{-2}, an upper limit to the reflection fraction of 0.35, and a cut-off energy of 80^{+50}_{-20} keV. The Fe Kα line has an equivalent width of 70 ± 30 eV. The temperature of the MEKAL component is found to be $0.15^{+0.04}_{-0.06}$ keV, while its normalization is $(9 \pm 4) \times 10^{-5}$. Finally, the scattered fraction is $(1.8 \pm 4) \times 10^{-2}$.

3.3.4 PKS 2331−240

NuSTAR observed this source in 2015 July with a net exposure of 24 ks; *XMM–Newton* observed the source twice, in 2015 May and November (Obs. IDs 0760990101 and 0760990201) with a net exposure of 18 and 20 ks, respectively. We first fitted the *NuSTAR* and pn spectra in the 3–10 keV band with a simple power law, finding a discrepancy between the different spectra. Indeed, we found a photon index of 1.81 ± 0.06 in *NuSTAR*, 1.72 ± 0.05 in the first pn spectrum and 1.64 ± 0.05 in the second pn spectrum. Moreover, the 3–10 keV flux in pn was found to be 20 and 30 per cent less than in *NuSTAR*. However, to constrain N_H and the Fe Kα line, we chose to include the pn spectra in our fits, leaving the photon index free to vary among the different observations. Since the BAT photon index was poorly constrained, we tied it to that of *NuSTAR*. We obtain a decent fit using Model A (χ^2/dof = 611/540), with residuals that can be attributed to noise. Albeit this source is optically an Sy1.9, it is almost unabsorbed (see also Hernández-García et al. 2017) and we only find a column density of $(1.1 \pm 0.3) \times 10^{20}$ cm^{-2} in excess of the Galactic one. We find an upper limit to the reflection fraction of 0.3 and an Fe Kα line with an equivalent width of 50 ± 20 eV. The *NuSTAR* photon index for the broad-band (0.3–195 keV) fit is 1.91 ± 0.07, while for pn we have 1.75 ± 0.02 and 1.77 ± 0.02 (consistent with Hernández-García et al. 2017) and a cross-calibration constant of 0.65 ± 0.07 and 0.54 ± 0.06, respectively.

3.3.5 PKS 2356−61

We fitted the *NuSTAR* and BAT spectra with Model A, which yields a decent fit (χ^2/dof = 131/159). We obtain a photon index of 1.7 ± 0.3 and a column density of $(1.4 \pm 0.5) \times 10^{23}$ cm^{-2}, in agreement with the results of Mingo et al. (2014) from *Chandra* data alone. We only derive upper limits to the presence of a reflection component ($\mathcal{R} < 1.3$) and of an Fe Kα line ($EW_{K\alpha} < 170$ eV).

4 DISCUSSION

4.1 X-ray properties

The X-ray spectral properties of the hard X-ray-selected GRGs of our sample are overall consistent with that of normal-size FR II radio galaxies, and more precisely of 'high-excitation' radio galaxies (HERGs) powered by efficient accretion (e.g. Hardcastle, Evans & Croston 2006; Hardcastle et al. 2009; Mingo et al. 2014). The X-ray spectra are generally well described by a power law with a photon index Γ_X in the range 1.6–1.9, i.e. typical of average AGNs (e.g. Malizia et al. 2014). In general, past observations have shown that spectral features such as the Compton hump and the Fe Kα line tend to be weaker in radio galaxies, compared with radio-quiet Seyferts (e.g. Wozniak et al. 1998; Eracleous, Sambruna & Mushotzky 2000; Grandi et al. 2001; Molina et al. 2008; Walton et al. 2013). From high-sensitivity measurements obtained in recent years with *NuSTAR*, a weak or absent reflection bump has been found in 3C 382 (Ballantyne et al. 2014; Ursini et al. 2018b), 3C 273 (Madsen et al. 2015), 3C 390.3 (Lohfink et al. 2015), and Cen A (Fürst et al. 2016); on the other hand, signatures of reflection (neutral or ionized) have been observed in 3C 120 (Lohfink et al. 2013), Cyg A (Reynolds et al. 2015), and 4C 74.26 (Lohfink et al. 2017), which is part of our sample. Although our results suggest a trend of weak reflection features, future studies on larger samples will be needed to properly estimate the contribution of the reflection component in radio galaxies. Interestingly, King, Lohfink & Kara (2017) reported an inverse correlation between the radio Eddington luminosity and the X-ray reflection fraction in a sample of AGNs, both radio quiet and radio loud. King et al. (2017) interpreted this result in terms of an outflowing, mildly relativistic corona, whose emission is beamed away from the accretion disc and the surrounding material (e.g. Beloborodov 1999; Malzac, Beloborodov & Poutanen 2001). This would be consistent with the X-ray corona being the base of the radio jet, as suggested for X-ray binaries (Markoff, Nowak & Wilms 2005) and radio galaxies like 3C 120 (Lohfink et al. 2013).

An exponential high-energy cut-off is measured in four sources out of 14, two of which have been analysed here (0318+684 and Mrk 1498). In three cases, we only derived lower limits to the cut-off based on *NuSTAR* data. The presence of a high-energy cut-off is consistent with the X-ray emission originating via thermal Comptonization rather than synchrotron and/or inverse Compton in a jet. We also note that none of our sources is a strong gamma-ray emitter, as they are not detected by *Fermi* (Acero et al. 2015); to our knowledge, the only exception is B3 0309+411b, for which Hooper,

Table 6. X-ray and radio energetic properties: column (2) 2–10 keV flux; column (3) 2–10 keV luminosity; column (4) core flux density at 1.4 GHz; column (5) lobes flux density at 1.4 GHz; column (6) core luminosity at 1.4 GHz; and column (7) lobes luminosity at 1.4 GHz.

Name	F(2–10 keV) (10^{-12} erg s^{-1} cm^{-2})	L(2–10 keV) (10^{43} erg s^{-1})	$S^{\rm core}_{\rm 1.4GHz}$ (mJy)	$S^{\rm lobes}_{\rm 1.4GHz}$ (mJy)	$L^{\rm core}_{\rm 1.4GHz}$ (10^{40} erg s^{-1})	$L^{\rm lobes}_{\rm 1.4GHz}$ (10^{40} erg s^{-1})
B3 0309+411b	2.4	13	379	141	25.6	9.5
0318+684	3.7	13.5	22	801	0.6	23
PKS 0707−35(a)	1.2	5	44.6	445.6	2	20.5
PKS 0707−35(b)				1455.4		67
4C 73.08	1.6	2.6	15.6	2521.4	0.18	28.6
HE 1434−1600	7.2	38	72	7068	5.7	564
IGR J14488−4008	5.3	25	58.2	276.6	3.3	15.6
4C 63.22	3.6	45	18.3	657.7	3.1	110
Mrk 1498	8.1	10	74	557	0.74	5.6
4C 34.47	8.5	93	610	980	106	171
IGR J17488−2338	2.0	42	60.5	337.1	14.9	83.3
PKS 2014−55	3.9	3.0	40	2560	0.49	31.3
4C 74.26	30.0	80	184	1621	7.1	62.6
PKS 2331−240	12.0	6	362	798	2.8	6.1
PKS 2356−61	2.7	11.5	16	24700	0.53	820

Linden & Lopez (2016) reported a 0.1–100 GeV flux $\simeq 2.5 \times 10^{-12}$ erg s^{-1} cm^{-2} from 85-month *Fermi* data. The lack of a strong gamma-ray emission indicates that a high-energy cut-off is likely present below the MeV band.

All in all, the X-ray emission is consistent with being accretion-related and possibly due to a hot Comptonizing corona, that could be outflowing. The jet component could give a significant contribution, at least in the soft X-ray band (Hardcastle et al. 2006, 2009), but is unlikely to dominate the overall emission in most sources (see also Mingo et al. 2017). In the case of PKS 2331−240, the X-ray emission is consistent with originating from external inverse Compton scattering in the jet (Hernández-García et al. 2017), but this is the only source of our sample classified as a blazar.

Finally, the X-ray absorption properties are in agreement with the zeroth-order predictions of unified models of AGNs (e.g. Antonucci 1993; Urry & Padovani 1995), as type 1 and 2 objects tend to be unobscured and obscured, respectively (for a detailed discussion on the full sample of hard X-ray-selected radio galaxies, see Panessa et al. 2016).

In Table 6, we report the X-ray (2–10 keV) flux and luminosity of all the 14 GRGs of our sample, and the radio (1.4 GHz) flux density and νL_ν luminosity of their core and lobes. The radio flux densities were mostly taken from the literature (see Tables 1 and 2). For IGR J14488−4008, we extrapolated to 1.4 GHz the Giant Metrewave Radio Telescope (*GMRT*) measurements at 325 and 610 MHz by Molina et al. (2015). For PKS 2014−55, the fluxes of the core and of the extended structures were estimated from the Australia Telescope Compact Array *(ATCA)* map (Saripalli et al. 2007). For PKS 2356−61, we extrapolated to 1.4 GHz, the 2.3- and 5-GHz measurements by Morganti, Killeen & Tadhunter (1993) and Morganti et al. (1997). In the case of PKS 0707−35, we reported the fluxes of the inner lobes (i) and outer lobes (ii) separately (Saripalli et al. 2013). A more detailed analysis of the radio properties of the sample will be developed in Bruni et al. (in preparation).

4.2 Radio–X-ray relation

A relationship is known to exist between the radio core luminosity, the X-ray luminosity and the black hole mass in AGNs and X-ray binaries (the so-called fundamental plane of black hole activity: Merloni, Heinz & di Matteo 2003; Falcke, Körding & Markoff 2004; Gültekin et al. 2009). The original relation of Merloni et al. (2003) is:

$$\log L^{\rm core}_{\rm 5GHz} = \xi_{\rm RX} \log L_{\rm 2-10keV} + \xi_{\rm RM} \log M + b_{\rm R} \quad (1)$$

with $\xi_{\rm RX} = 0.6$, $\xi_{\rm RM} = 0.78$, and $b_{\rm R} = 7.33$. In Fig. 1, we plot the radio luminosity $L^{\rm core}_{\rm 1.4GHz}$ against the X-ray luminosity $L_{\rm 2-10keV}$ for our sources. We performed a linear regression fit in the logarithmic

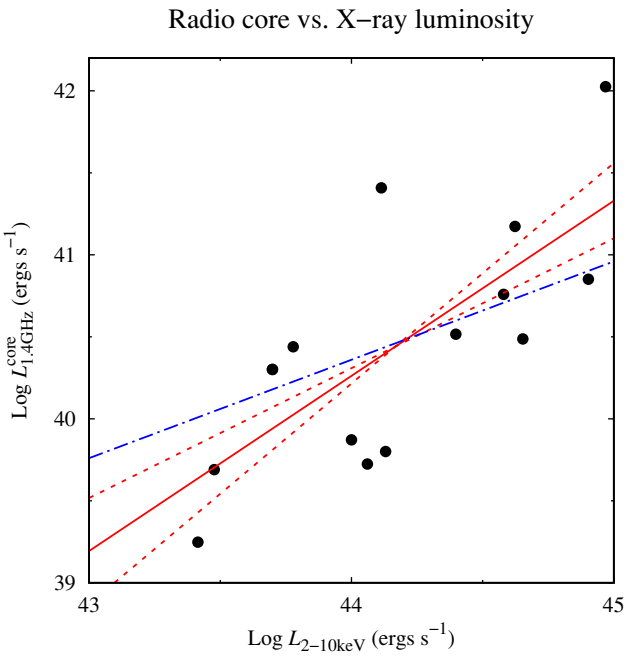

Figure 1. Radio core 1.4-GHz luminosity versus X-ray 2–10 keV luminosity. The red solid line represents a linear fit in the log–log space, while the red dashed lines correspond to the 90 per cent error on the slope and normalization. The blue dotted–dashed line represents the relation of Merloni et al. (2003) for a black hole mass of 10^8 solar masses.

space:

$$\log L^{\rm core}_{1.4{\rm GHz}} = \xi_{\rm RX} \log L_{2-10{\rm keV}} + C \quad (2)$$

finding $\xi_{\rm RX} = 1.1 \pm 0.3$ and $C = -7 \pm 12$. The linear correlation is significant, as we calculate a Kendall's coefficient $\tau = 0.63$ with a p-value of 1×10^{-3}. However, to properly evaluate the significance of this correlation, we need to take into account the uncertainty on the X-ray and radio luminosities. In principle, both measurement errors and flux variability can contribute to this uncertainty. However, the measurement errors are generally small, i.e. no more than a few per cent; flux variability, on the other hand, can easily amount up to a factor of a few. In particular, the X-ray variability in our sources can be up to 0.3 dex as indicated by the cross-calibration constants of our fits (see Table 4). Taking 0.3 dex as a fiducial uncertainty on $L_{2-10{\rm keV}}$ and $L^{\rm core}_{1.4{\rm GHz}}$, we performed a bootstrap on the data, finding a 99 per cent confidence interval for the Kendall's coefficient of $0.15 < \tau < 0.95$. Finally, we tested for a possible distance effect on the correlation, namely the bias introduced by the common dependence of $L_{2-10{\rm keV}}$ and $L^{\rm core}_{1.4{\rm GHz}}$ on the distance (e.g. Merloni et al. 2006). We thus performed a partial Kendall's correlation test among $L^{\rm core}_{1.4{\rm GHz}}$ and $L_{2-10{\rm keV}}$, using the luminosity distance as the third variable. We obtained $\tau = 0.42$ with a p-value of 4×10^{-2}, i.e. still a significant correlation. Also in this case, we performed a bootstrap on the data, assuming an uncertainty on the distance of 0.4 dex due to the uncertainty on the Hubble flow (Körding, Falcke & Corbel 2006). We obtained a 99 per cent confidence interval for the Kendall's coefficient of $0.15 < \tau < 0.68$.

In Fig. 1, we overplot the relation of Merloni et al. (2003) converting the 5-GHz luminosity into the 1.4-GHz luminosity assuming a radio spectral index $\alpha = 0.7$, where $L_\nu \propto \nu^{-\alpha}$ (Condon, Cotton & Broderick 2002), and a black hole mass of 10^8 solar masses. We note that the estimates of the black hole mass are available only in eight sources out of 14 (i.e. the brightest, see Panessa et al. 2016). This uncertainty, coupled with the intrinsic scatter about the fundamental plane, could explain the discrepancy among the data and the relation of Merloni et al. (2003), also given the limited size of our sample. We also note that different estimates of the fundamental plane have been reported, using larger samples (e.g. Körding et al. 2006; Li, Wu & Wang 2008; Bonchi et al. 2013). However, our results are consistent with previous findings by Panessa et al. (2015), who analysed the 1.4-GHz radio properties of a complete sample of hard X-ray-selected AGNs, reporting a steep radio–X-ray correlation ($\xi_{\rm RX} \simeq 1$). It is thus possible that the hard X-ray GRGs belong to a different branch in the radio–X-ray correlation. The physical meaning of the fundamental plane is the existence of a relationship between accretion power and jet emission (e.g. Hardcastle et al. 2009), both in AGNs and in Galactic X-ray binaries (e.g. Gallo, Fender & Pooley 2003). Although the underlying mechanism of this coupling is still a matter of speculation, it might suggest that the X-ray emitting corona is the base of the jet (e.g. Markoff et al. 2005). However, alternative models exist, like the so-called jet emitting discs in X-ray binaries (Ferreira et al. 2006; Petrucci et al. 2010). Furthermore, X-ray binaries seem to exhibit two different branches in the radio–X-ray correlation: the 'standard' branch with $\xi_{\rm RX} \simeq 0.6$, and a second branch with $\xi_{\rm RX} \simeq 1-1.4$ (Coriat et al. 2011; Gallo, Miller & Fender 2012). The first branch is consistent with the source being powered by a radiatively inefficient accretion flow, in which most of the released energy is advected (Narayan & Yi 1994) and/or channelled into outflows (Blandford & Begelman 1999) or jets (Markoff et al. 2005). The second branch is instead consistent with radiatively efficient flows, like the standard Shakura & Sunyaev (1973) accretion disc or the jet-emitting disc (Ferreira et al. 2006). Extrapolating these results to AGNs, the hard X-ray-selected GRGs would be located in the 'efficient' branch of the radio–X-ray diagram, since $\xi_{\rm RX} \simeq 1.1$. This in turn suggests that their nuclear activity is driven by a radiatively efficient mode of accretion, with the caveat that several uncertainties remain on the nature of the 'efficient' branch, complicating the theoretical interpretation (Gallo et al. 2012, but see also Motta, Casella & Fender 2018).

4.3 Bolometric luminosity

In radio galaxies, the radio luminosity of the lobes is found to be related with the disc luminosity (e.g. Willott et al. 1999; Körding, Jester & Fender 2008; van Velzen & Falcke 2013; van Velzen, Falcke & Körding 2015). In particular, van Velzen et al. (2015) reported a linear correlation, in the logarithmic space, between the 1.4-GHz lobes luminosity and the bolometric luminosity estimated from the optical one; the normalization is

$$\log(L^{\rm lobes}_{1.4{\rm GHz}}/L_{\rm bol}) = -3.57. \quad (3)$$

We used this relation to estimate the bolometric luminosity from $L^{\rm lobes}_{1.4{\rm GHz}}$. This estimate is labelled $L^{\rm radio}_{\rm bol}$ in the following. The major source of uncertainty on $L^{\rm radio}_{\rm bol}$ is the scatter of the van Velzen et al. (2015) relation, amounting to 0.47 dex (rms).

The bolometric luminosity can be independently estimated from the X-ray 2–10 keV luminosity using bolometric corrections (e.g. Marconi et al. 2004; Hopkins, Richards & Hernquist 2007; Runnoe, Brotherton & Shang 2012). Assuming the Marconi et al. (2004) correction, we computed the bolometric luminosity $L^{\rm X}_{\rm bol}$. This quantity is directly related to the present nuclear activity, while $L^{\rm radio}_{\rm bol}$ can be viewed as a tracer of the past activity. Because the scatter of the Marconi et al. (2004) relation is $\sim$0.1 dex, the main source of uncertainty on $L^{\rm X}_{\rm bol}$ is the X-ray flux variability, which increases the spread in any bolometric correction (Vasudevan & Fabian 2007). We also note that assuming a different bolometric correction would yield estimates of $L^{\rm X}_{\rm bol}$ within a factor of a few. For example, the linear correction of Runnoe et al. (2012) for radio-loud AGNs yields estimates within a factor of $\sim$3, while the luminosity-dependent correction of Hopkins et al. (2007) yields systematically larger estimates of $L^{\rm X}_{\rm bol}$ up to a factor of 2. We also checked that the estimates of $L^{\rm X}_{\rm bol}$ are in rough agreement, again within a factor of a few, with the constant correction of Mushotzy et al. (2008) for the 14–195 keV luminosity, and with the Eddington ratio-dependent correction of Vasudevan & Fabian (2009). However, we stress that our main purpose is only to compare the AGN luminosity as traced by the X-ray emission with the luminosity as inferred by the radio lobes.

In Fig. 2, we plot the two independent estimates of the bolometric luminosity. Most of the objects exhibit a discrepancy between $L^{\rm radio}_{\rm bol}$ and $L^{\rm X}_{\rm bol}$, $L^{\rm radio}_{\rm bol}$ being around one order of magnitude smaller than $L^{\rm X}_{\rm bol}$. Despite all the aforementioned uncertainties, the discrepancy between $L^{\rm radio}_{\rm bol}$ and $L^{\rm X}_{\rm bol}$ is significant, at least in nine sources out of 14. Interestingly, this discrepancy is consistent with a similar trend seen in blazars with double radio lobes (Pjanka, Zdziarski & Sikora 2017). Indeed, Pjanka et al. (2017) found that the blazar jet powers measured from radio lobes are a factor of $\sim$10 lower than those from blazar-model spectral fitting (Ghisellini et al. 2014) or from the angular shift of the radio core (Zdziarski et al. 2015). Pjanka et al. (2017) proposed two different explanations for this discrepancy. First, it could be a signature of intermittent accretion. In this case, luminous and efficient quasars ($\varepsilon_{\rm Edd} \gtrsim 0.03$) could be caught in a

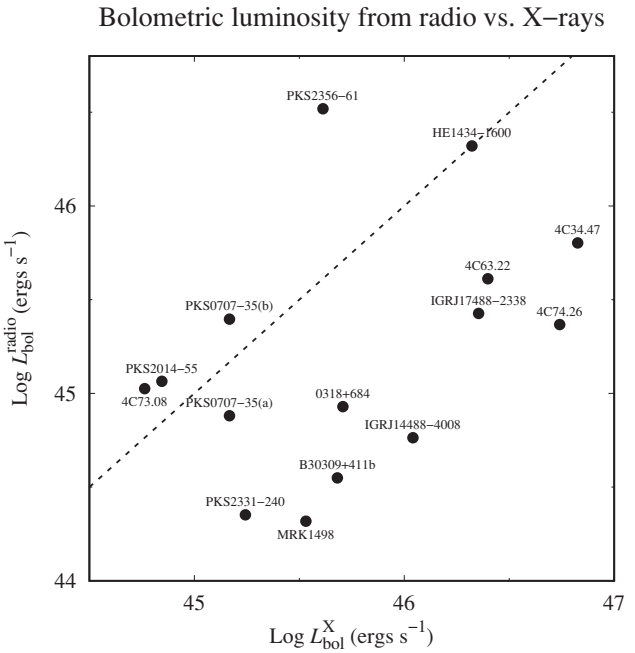

Figure 2. Bolometric luminosity estimated from the radio luminosity of the lobes (y-axis) versus that estimated from the 2–10 keV luminosity (x-axis). The dashed line represents the identity $y = x$.

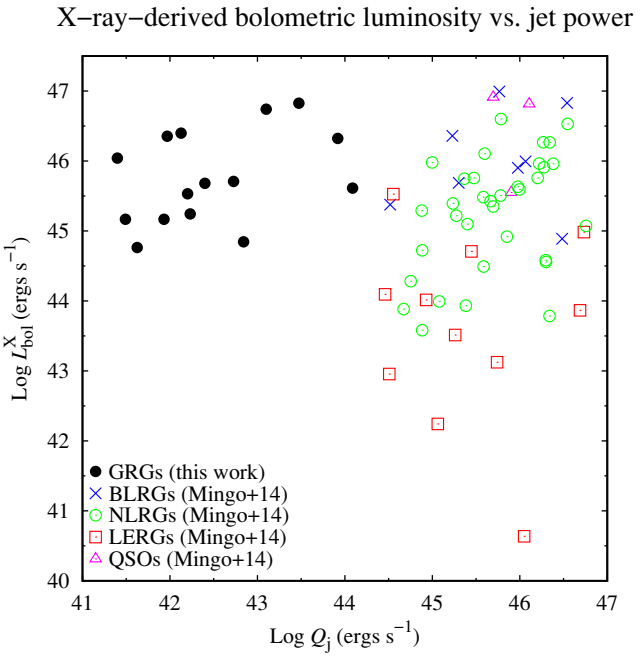

Figure 3. Bolometric luminosity estimated from the 2–10 keV luminosity versus jet power estimated from the relation of Willott et al. (1999). Black dots denote the GRGs of our sample, overlayed in the plot of Mingo et al. (2014).

high state lasting only a small fraction of the entire lifetime, which is mostly spent in quiescent states (see also van Velzen & Falcke 2013). Alternatively, the jet power from the blazar model could be overestimated due to the presence of $e^{\pm}$ pairs (see also Sikora 2016). In our case, we observe a discrepancy between the nuclear luminosity, traced by the X-rays, and the radio lobes luminosity, estimated from the disc–lobes relationship reported by van Velzen et al. (2015) for radio-selected FR IIs. This could mean that the van Velzen et al. (2015) relationship may not hold for the GRGs in our sample. This in turn suggests that either their nuclear luminosity is higher than the average luminosity during their lifetime, or that their lobes luminosity is lower than expected (possibly due to radiative losses). The former hypothesis could point to an intermittent activity scenario, as we discuss in the next sections. However, we cannot exclude that the correlation of van Velzen et al. (2015) is affected by sample selection effects, since different studies have found wider ranges of radio luminosities, or jet powers, for a given accretion-related luminosity, e.g. in the optical (Mingo et al. 2014) or mid-infrared (Gürkan, Hardcastle & Jarvis 2014). Therefore, the estimate L_{bol}^{radio} should not to be overinterpreted (see also Hardcastle 2018; Croston, Ineson & Hardcastle 2018). Still, it is remarkable that a similar result is obtained, with independent methods, both in blazars and in GRGs, i.e. two classes vastly different in physical size and jet orientation. In the next section, we will also show that the estimated jet power is much lower than in radio luminous radio galaxies.

Finally, for the sources having estimates of the black hole mass, we can also estimate the Eddington ratio as the ratio between the bolometric luminosity L_{bol}^{X} and the Eddington luminosity. In seven sources out of eight, we estimate Eddington ratios between 0.02 and 0.37, i.e. consistent with the typical values found in efficient HERGs (Best & Heckman 2012; Mingo et al. 2014). For 4C 34.47, we obtain an Eddington ratio of ∼5, which could indicate that the bolometric luminosity is overpredicted, and/or that the black hole mass is underestimated (1×10^8 $M_\odot$ according to Liu, Jiang & Gu 2006, single-epoch estimate based on the Hβ line).

4.4 Jet power

The time-averaged kinetic power of AGN jets can be estimated from the extended radio luminosity[2] (Willott et al. 1999; Cavagnolo et al. 2010). We estimated the jet power Q_j using the relationship obtained by Willott et al. (1999), based on the minimum energy required in the lobes to produce the observed synchrotron luminosity and the evolution of the radio source. In particular, we used equation (12) of Willott et al. (1999):

$$Q_j = 3 \times 10^{38} \mathcal{L}_{151}^{6/7} \mathrm{W} \quad (4)$$

where $\mathcal{L}_{151}$ is the luminosity at 151 MHz in units of 10^{28} W Hz^{-1} sr^{-1}. The uncertainties in the model assumptions are enclosed in a factor f, expected to be in the range 1–20, where Q_j depends on $f^{3/2}$. In principle, this would imply a systematic uncertainty up to two orders of magnitude in jet power for a given radio luminosity (see also Godfrey & Shabala 2013). However, the scatter in the radio power/jet power relation is much lower, both from direct measurements (Godfrey & Shabala 2013) and numerical simulations (at least for sources in a narrow redshift band, see Hardcastle 2018). In any case, the relation is useful to probe the efficiency of jet production in different classes of AGNs, as done by Mingo et al. (2014). In Fig. 3, we plot the X-ray-derived bolometric luminosity L_{bol}^{X} against the jet power. Our GRGs are added on to the plot of the sample of bright radio galaxies of Mingo et al. (2014), selected combining

[2]To this goal, we converted the 1.4-GHz luminosity into the 151-MHz luminosity assuming a spectral index of 0.7.

the 2 Jy catalogue (Wall & Peacock 1985) with the 3CRR catalogue (Laing et al. 1983). We note that Mingo et al. (2014), like us, assumed the Marconi et al. (2004) bolometric correction and the Willott et al. (1999) relation to derive L^{X}_{bol} and Q_j, respectively. For simplicity, we plot only the sources of the Mingo et al. (2014) sample with a well-constrained L^{X}_{bol} (see their fig. 12). Following Mingo et al. (2014), we highlight different optical classes: broad-line radio galaxies (BLRGs), narrow-line radio galaxies (NLRGs), low-excitation radio galaxies (LERGs), and quasars.

From Fig. 3, it can be seen that the X-ray-derived bolometric luminosity of the GRGs of our sample is consistent with that of HERGs (namely BLRGs, NLRGs, and quasars) in the Mingo et al. (2014) sample. On the other hand, the estimated jet power of our GRGs is found to be down to $\sim 10^{42}$ erg s^{-1}, and much lower than that of the sources of Mingo et al. (2014). This is not totally unexpected, because the sources of Mingo et al. (2014) are by construction the most radio luminous in the Universe, implying the highest jet powers. However, the difference with our GRGs can be very large, up to 3 orders of magnitude in jet power. Moreover, Mingo et al. (2014) also compared their sample with an optically selected sample of radio-loud quasars (Punsly & Zhang 2011), and even those sources have an estimated $Q_j > 10^{43}$ erg s^{-1}. Therefore, the interpretation of our results is not straightforward. First, the (unknown) environment and source age can strongly affect the estimate of the jet power (e.g. Shabala & Godfrey 2013; Hardcastle 2018). Giant sources might have undergone severe radiative losses compared with normal-size radio galaxies, which could explain the relatively small inferred jet power. In other words, any relation between accretion power and ejection at small scales (i.e. the radio core) could be completely lost as the source grows in size, due to radiative losses and complex interaction with the environment. Then, in a luminosity–luminosity diagram like that of Fig. 3, GRGs in the early stage of their life could well start in the upper right part (i.e. high nuclear luminosities/high jet powers) and move to the left-hand side at later times. If in most sources, the central engine gradually fades (and eventually switches off), most of radio-selected GRGs would be expected to populate the lower part of the plot (i.e. low nuclear luminosities). Hard X-ray selection instead picks the GRGs with a high nuclear luminosity. These could be sources that are able to keep a more or less constant nuclear power during their life (so they just shift horizontally along the diagram), or that experienced one or more episodes of restarting activity.

4.5 Restarting activity?

A number of radio galaxies are known to exhibit signatures of restarting activity, from their morphological and/or spectral radio properties (Saikia & Jamrozy 2009, and references therein). A striking evidence of restarting activity is seen in the so-called double–double radio galaxies, which exhibit two distinct pairs of radio lobes: a 'new' one, closer to the core, and an 'old' one, farther away (e.g. Schoenmakers et al. 2000b). Among our sample, PKS 0707−35 is a clear example of a restarted radio galaxy (Saripalli et al. 2013). PKS 2014−55 is also a restarted GRG with an X-shaped morphology that could be a signature of jet reorientation (Saripalli et al. 2007). An extreme case of jet realignment is PKS 2331−240, that switched from a double-lobe GRG to a blazar (Hernández-García et al. 2017). Other hints of restarting jet activity have been found in 4C 73.08, that displays an extended radio cocoon around the brighter lobes (Weżgowiec et al. 2016). Concerning the spectral properties, some GRGs show a gigahertz-peaked spectrum core, which is generally associated with young and compact radio sources at the early stage of their evolution (e.g. O'Dea 1998). This suggests that the core emission is relatively recent, despite the old age of the lobes. Among our sample, this is seen at least in 0318+684 (Schoenmakers et al. 1998) and 4C 74.26 (Pearson et al. 1992). A detailed discussion will be presented in Bruni et al. (in preparation), showing that signatures of restarting activity are found in at least 11 sources out of 14, i.e. 80 per cent of the sample. The restarting activity scenario is an intriguing possibility to explain the properties of hard X-ray-selected GRGs. On the one hand, the correlation between radio cores and X-ray emission indicates the existence of a physical relationship between the inner jet at pc scales and the X-ray-emitting region. On the other hand, the jet power and the luminosity of the radio lobes in most sources is less than expected from the nuclear luminosity. Therefore, the sources could be in a restarting phase, characterized by efficient accretion and a high nuclear activity.

Although hard X-ray selection favours the detection of giant objects, no correlation is found between the X-ray luminosity and the source size, consistent with the idea that more than one parameter is involved in the production of large-scale radio structures (Bassani et al. 2016). One of such parameters could be the duty cycle. The intermittency of fuel supply can occur on different time-scales, and has been assumed to explain the optical properties of weak-line radio galaxies (Tadhunter 2016, and references therein). If the accretion mechanism in AGNs and black hole X-ray binaries is the same, as suggested by the fundamental plane, then we expect AGNs to undergo dramatic changes of the accretion state like those seen in X-ray binaries (e.g. Maccarone, Gallo & Fender 2003). Given their old age, GRGs offer chances to witness such variations and constrain scenarios of episodic activity. Alternatively, if the nuclear activity does not change dramatically over time, the observed dimming of the radio lobes could be due to expansion losses. In particular, the inverse Compton scattering of the cosmic microwave background is expected to dominate in giant sources (e.g. Ishwara-Chandra & Saikia 1999; Laskar et al. 2010; Hardcastle 2018). This would lead us to the prediction that the intrinsic fraction of GRGs is much larger than that found in present radio surveys, being greater than the 20 per cent found from hard X-ray selection (including relict sources not seen in the X-rays and not currently fed by the jet; see Saripalli et al. 2005). However, in this case, the nuclei are required to stay continuously active for around 100–250 Myr, as indicated by the typical dynamical ages estimated for GRGs (Machalski 2011).

5 SUMMARY

We have presented the first broad-band X-ray study of the nuclei of a sample of 14 hard X-ray-selected GRGs, from the literature and the analysis of archival X-ray data. Our main conclusions can be summarized as follows:

(1) The X-ray properties of hard X-ray-selected GRGs are analogous to that of normal-size FR II radio galaxies. The X-ray photon index is generally consistent with that of radio-quiet AGNs, and a high-energy cut-off is measured in four sources. The bulk of the X-ray emission is generally consistent with originating from a Comptonizing corona, possibly outflowing, coupled to a radiatively efficient accretion flow ($\varepsilon_{Edd} > 0.02$).

(2) The X-ray luminosity correlates with the radio core luminosity, as expected from the fundamental plane of black hole activity for AGNs and X-ray binaries. However, the relationship is consistent with the 'radiatively efficient' branch of the radio–X-ray correlation rather than the 'standard/inefficient' branch, consistently with the optical HERG classification.

(3) The radio luminosity of the lobes is relatively low compared with the nuclear luminosity, as also indicated by the estimate of the jet kinetic power. This can be explained by restarting activity (i.e. the sources are currently highly accreting and in a high-luminosity state compared with the past activity that produced the old and extended radio lobes) and/or by a significant dimming of the radio lobes due to expansion losses.

ACKNOWLEDGEMENTS

We thank the referee for useful comments that improved the paper. We acknowledge the use of public data from the *NuSTAR*, *XMM–Newton*, *Swift*, and *INTEGRAL* data archives. This research has made use of data, software and/or web tools obtained from NASA's High Energy Astrophysics Science Archive Research Center, a service of Goddard Space Flight Center and the Smithsonian Astrophysical Observatory, and of the *NuSTAR* Data Analysis Software jointly developed by the ASI Space Science Data Center (Italy) and the California Institute of Technology (USA). We acknowledge financial support from ASI under contracts ASI/INAF 2013-025-R0 and ASI/INAF I/037/12/0 (NARO18).

REFERENCES

Acero F. et al., 2015, ApJS, 218, 23
Anders E., Grevesse N., 1989, Geochim. Cosmochim. Acta, 53, 197
Antonucci R., 1993, ARA&A, 31, 473
Arnaud K. A., 1996, in Jacoby G. H., Barnes J., eds, ASP Conf. Ser. Vol. 101, Astronomical Data Analysis Software and Systems V. Astron. Soc. Pac., San Francisco, p. 17
Ballantyne D. R. et al., 2014, ApJ, 794, 62
Balmaverde B., Capetti A., Grandi P., 2006, A&A, 451, 35
Barthelmy S. D. et al., 2005, Space Sci. Rev., 120, 143
Bassani L., Venturi T., Molina M., Malizia A., Dallacasa D., Panessa F., Bazzano A., Ubertini P., 2016, MNRAS, 461, 3165
Baumgartner W. H., Tueller J., Markwardt C. B., Skinner G. K., Barthelmy S., Mushotzky R. F., Evans P. A., Gehrels N., 2013, ApJS, 207, 19
Beloborodov A. M., 1999, ApJ, 510, L123
Best P. N., Heckman T. M., 2012, MNRAS, 421, 1569
Bird A. J. et al., 2010, ApJS, 186, 1
Blandford R. D., Begelman M. C., 1999, MNRAS, 303, L1
Bonchi A., La Franca F., Melini G., Bongiorno A., Fiore F., 2013, MNRAS, 429, 1970
Cavagnolo K. W., McNamara B. R., Nulsen P. E. J., Carilli C. L., Jones C., Bîrzan L., 2010, ApJ, 720, 1066
Condon J. J., Cotton W. D., Broderick J. J., 2002, AJ, 124, 675
Coriat M. et al., 2011, MNRAS, 414, 677
Croston J. H., Ineson J., Hardcastle M. J., 2018, MNRAS, 476, 1614
Di Gesu L., Costantini E., 2016, A&A, 594, A88
Eguchi S., Ueda Y., Terashima Y., Mushotzky R., Tueller J., 2009, ApJ, 696, 1657
Eracleous M., Sambruna R., Mushotzky R. F., 2000, ApJ, 537, 654
Falcke H., Körding E., Markoff S., 2004, A&A, 414, 895
Fanaroff B. L., Riley J. M., 1974, MNRAS, 167, 31P
Ferreira J., Petrucci P.-O., Henri G., Saugé L., Pelletier G., 2006, A&A, 447, 813
Fürst F. et al., 2016, ApJ, 819, 150
Gallo E., Fender R. P., Pooley G. G., 2003, MNRAS, 344, 60
Gallo E., Miller B. P., Fender R., 2012, MNRAS, 423, 590
George I. M., Fabian A. C., 1991, MNRAS, 249, 352
Ghisellini G., Haardt F., Matt G., 1994, MNRAS, 267, 743
Ghisellini G., Tavecchio F., Maraschi L., Celotti A., Sbarrato T., 2014, Nature, 515, 376
Godfrey L. E. H., Shabala S. S., 2013, ApJ, 767, 12
Grandi P., Maraschi L., Urry C. M., Matt G., 2001, ApJ, 556, 35
Grandi P., Malaguti G., Fiocchi M., 2006, ApJ, 642, 113
Guainazzi M., Bianchi S., 2007, MNRAS, 374, 1290
Guainazzi M., Matt G., Perola G. C., 2005, A&A, 444, 119
Gültekin K., Cackett E. M., Miller J. M., Di Matteo T., Markoff S., Richstone D. O., 2009, ApJ, 706, 404
Gürkan G., Hardcastle M. J., Jarvis M. J., 2014, MNRAS, 438, 1149
Haardt F., Maraschi L., 1991, ApJ, 380, L51
Haardt F., Maraschi L., Ghisellini G., 1994, ApJ, 432, L95
Haardt F., Maraschi L., Ghisellini G., 1997, ApJ, 476, 620
Hardcastle M. J., 2018, MNRAS, 475, 2768
Hardcastle M. J., Krause M. G. H., 2013, MNRAS, 430, 174
Hardcastle M. J., Evans D. A., Croston J. H., 2006, MNRAS, 370, 1893
Hardcastle M. J., Evans D. A., Croston J. H., 2009, MNRAS, 396, 1929
Harrison F. A. et al., 2013, ApJ, 770, 103
Hernández-García L. et al., 2017, A&A, 603, A131
Hernández-García L. et al., 2018, MNRAS, 478, 4634
Hooper D., Linden T., Lopez A., 2016, J. Cosmol. Astropart. Phys., 8, 019
Hopkins P. F., Richards G. T., Hernquist L., 2007, ApJ, 654, 731
Ishwara-Chandra C. H., Saikia D. J., 1999, MNRAS, 309, 100
Jagers W. J., Miley G. K., van Breugel W. J. M., Schilizzi R. T., Conway R. G., 1982, A&A, 105, 278
Jansen F. et al., 2001, A&A, 365, L1
Kaiser C. R., Alexander P., 1999, MNRAS, 302, 515
Kalberla P. M. W., Burton W. B., Hartmann D., Arnal E. M., Bajaja E., Morras R., Pöppel W. G. L., 2005, A&A, 440, 775
Keel W. C. et al., 2015, AJ, 149, 155
Keel W. C. et al., 2017, ApJ, 835, 256
King A. L., Lohfink A., Kara E., 2017, ApJ, 835, 226
Körding E., Falcke H., Corbel S., 2006, A&A, 456, 439
Körding E. G., Jester S., Fender R., 2008, MNRAS, 383, 277
Laing R. A., Riley J. M., Longair M. S., 1983, MNRAS, 204, 151
Lara L., Cotton W. D., Feretti L., Giovannini G., Marcaide J. M., Márquez I., Venturi T., 2001, A&A, 370, 409
Laskar T., Fabian A. C., Blundell K. M., Erlund M. C., 2010, MNRAS, 401, 1500
Letawe G., Courbin F., Magain P., Hilker M., Jablonka P., Jahnke K., Wisotzki L., 2004, A&A, 424, 455
Li Z.-Y., Wu X.-B., Wang R., 2008, ApJ, 688, 826
Liu Y., Jiang D. R., Gu M. F., 2006, ApJ, 637, 669
Lohfink A. M. et al., 2013, ApJ, 772, 83
Lohfink A. M. et al., 2015, ApJ, 814, 24
Lohfink A. M. et al., 2017, ApJ, 841, 80
Maccarone T. J., Gallo E., Fender R., 2003, MNRAS, 345, L19
Machalski J., 2011, MNRAS, 413, 2429
Machalski J., Chyzy K. T., Jamrozy M., 2004, AcA, 54, 249
Mack K.-H., Klein U., O'Dea C. P., Willis A. G., Saripalli L., 1998, A&A, 329, 431
Madsen K. K. et al., 2015, ApJ, 812, 14
Magdziarz P., Zdziarski A. A., 1995, MNRAS, 273, 837
Malarecki J. M., Staveley-Smith L., Saripalli L., Subrahmanyan R., Jones D. H., Duffy A. R., Rioja M., 2013, MNRAS, 432, 200
Malarecki J. M., Jones D. H., Saripalli L., Staveley-Smith L., Subrahmanyan R., 2015, MNRAS, 449, 955
Malizia A., Bassani L., Bazzano A., Bird A. J., Masetti N., Panessa F., Stephen J. B., Ubertini P., 2012, MNRAS, 426, 1750
Malizia A., Molina M., Bassani L., Stephen J. B., Bazzano A., Ubertini P., Bird A. J., 2014, ApJ, 782, L25
Malzac J., Beloborodov A. M., Poutanen J., 2001, MNRAS, 326, 417
Marconi A., Risaliti G., Gilli R., Hunt L. K., Maiolino R., Salvati M., 2004, MNRAS, 351, 169
Markoff S., Nowak M. A., Wilms J., 2005, ApJ, 635, 1203
Matt G., Perola G. C., Piro L., 1991, A&A, 247, 25
Matt G., Guainazzi M., Maiolino R., 2003, MNRAS, 342, 422
Merloni A., Heinz S., di Matteo T., 2003, MNRAS, 345, 1057
Merloni A., Körding E., Heinz S., Markoff S., Di Matteo T., Falcke H., 2006, New Astron., 11, 567

Mingo B., Hardcastle M. J., Croston J. H., Dicken D., Evans D. A., Morganti R., Tadhunter C., 2014, MNRAS, 440, 269
Mingo B. et al., 2017, MNRAS, 470, 2762
Molina M. et al., 2008, MNRAS, 390, 1217
Molina M., Bassani L., Malizia A., Stephen J. B., Bird A. J., Bazzano A., Ubertini P., 2013, MNRAS, 433, 1687
Molina M., Bassani L., Malizia A., Bird A. J., Bazzano A., Ubertini P., Venturi T., 2014, A&A, 565, A2
Molina M., Venturi T., Malizia A., Bassani L., Dallacasa D., Lal D. V., Bird A. J., Ubertini P., 2015, MNRAS, 451, 2370
Morganti R., Killeen N. E. B., Tadhunter C. N., 1993, MNRAS, 263, 1023
Morganti R., Oosterloo T. A., Reynolds J. E., Tadhunter C. N., Migenes V., 1997, MNRAS, 284, 541
Motta S. E., Casella P., Fender R. P., 2018, MNRAS, 478, 5159
Mushotzy R. F., Winter L. M., McIntosh D. H., Tueller J., 2008, ApJ, 684, L65
Narayan R., Yi I., 1994, ApJ, 428, L13
O'Dea C. P., 1998, PASP, 110, 493
Oh K. et al., 2018, ApJS, 235, 4
Panessa F. et al., 2015, MNRAS, 447, 1289
Panessa F. et al., 2016, MNRAS, 461, 3153
Parisi P. et al., 2012, A&A, 545, A101
Pearson T. J., Blundell K. M., Riley J. M., Warner P. J., 1992, MNRAS, 259, 13P
Petrucci P. O., Ferreira J., Henri G., Malzac J., Foellmi C., 2010, A&A, 522, A38
Piconcelli E., Jimenez-Bailón E., Guainazzi M., Schartel N., Rodríguez-Pascual P. M., Santos-Lleó M., 2004, MNRAS, 351, 161
Pjanka P., Zdziarski A. A., Sikora M., 2017, MNRAS, 465, 3506
Punsly B., Zhang S., 2011, ApJ, 735, L3
Reynolds C. S. et al., 2015, ApJ, 808, 154
Ricci C. et al., 2017, ApJS, 233, 17
Runnoe J. C., Brotherton M. S., Shang Z., 2012, MNRAS, 422, 478
Saikia D. J., Jamrozy M., 2009, Bull. Astron. Soc. India, 37, 63
Saripalli L., Subrahmanyan R., 2009, ApJ, 695, 156
Saripalli L., Hunstead R. W., Subrahmanyan R., Boyce E., 2005, AJ, 130, 896
Saripalli L., Subrahmanyan R., Laskar T., Koekemoer A., 2007, in proceedings of "From planets to dark energy: the modern radio Universe" , PoS (MRU), 130
Saripalli L., Subrahmanyan R., Thorat K., Ekers R. D., Hunstead R. W., Johnston H. M., Sadler E. M., 2012, ApJS, 199, 27
Saripalli L., Malarecki J. M., Subrahmanyan R., Jones D. H., Staveley-Smith L., 2013, MNRAS, 436, 690
Schoenmakers A. P., Mack K.-H., Lara L., Röttgering H. J. A., de Bruyn A. G., van der Laan H., Giovannini G., 1998, A&A, 336, 455
Schoenmakers A. P., Mack K.-H., de Bruyn A. G., Röttgering H. J. A., Klein U., van der Laan H., 2000a, A&AS, 146, 293
Schoenmakers A. P., de Bruyn A. G., Röttgering H. J. A., van der Laan H., Kaiser C. R., 2000b, MNRAS, 315, 371
Shabala S. S., Godfrey L. E. H., 2013, ApJ, 769, 129
Shakura N. I., Sunyaev R. A., 1973, A&A, 24, 337
Sikora M., 2016, Galaxies, 4, 12
Subrahmanyan R., Saripalli L., Hunstead R. W., 1996, MNRAS, 279, 257
Tadhunter C., 2016, A&AR, 24, 10
Tazaki F., Ueda Y., Terashima Y., Mushotzky R. F., Tombesi F., 2013, ApJ, 772, 38
Turner T. J., George I. M., Nandra K., Mushotzky R. F., 1997, ApJS, 113, 23
Ubertini P. et al., 2003, A&A, 411, L131
Ueda Y. et al., 2007, ApJ, 664, L79
Urry C. M., Padovani P., 1995, PASP, 107, 803
Ursini F., Bassani L., Panessa F., Bazzano A., Bird A. J., Malizia A., Ubertini P., 2018a, MNRAS, 474, 5684
Ursini F. et al., 2018b, MNRAS, 478, 2663
van Velzen S., Falcke H., 2013, A&A, 557, L7
van Velzen S., Falcke H., Körding E., 2015, MNRAS, 446, 2985
Vasudevan R. V., Fabian A. C., 2007, MNRAS, 381, 1235
Vasudevan R. V., Fabian A. C., 2009, MNRAS, 392, 1124
Verner D. A., Ferland G. J., Korista K. T., Yakovlev D. G., 1996, ApJ, 465, 487
Véron-Cetty M.-P., Véron P., 2006, A&A, 455, 773
Wall J. V., Peacock J. A., 1985, MNRAS, 216, 173
Walton D. J., Nardini E., Fabian A. C., Gallo L. C., Reis R. C., 2013, MNRAS, 428, 2901
Wężgowiec M., Jamrozy M., Mack K.-H., 2016, Acta Astron., 66, 85
Willott C. J., Rawlings S., Blundell K. M., Lacy M., 1999, MNRAS, 309, 1017
Winter L. M., Mushotzky R. F., Tueller J., Markwardt C., 2008, ApJ, 674, 686
Wozniak P. R., Zdziarski A. A., Smith D., Madejski G. M., Johnson W. N., 1998, MNRAS, 299, 449
Zdziarski A. A., Sikora M., Pjanka P., Tchekhovskoy A., 2015, MNRAS, 451, 927

This paper has been typeset from a TEX/LATEX file prepared by the author.